DATA REPOSITORY ITEMS

Sample Locations

Sample Number	*Latitude**	*Longitude**
WR104	41º 28’ 27”	120º 11’ 11”
WR122	41º 24’ 10”	120º 09’ 24”

**North American Datum of 1983*

Apatite fission-track analysis: Methods and data

Samples were prepared and analyzed by J. Colgan at Stanford University. Apatite concentrates were prepared using standard mineral separation techniques, including crushing, grinding, Frantz magnetic separation, and heavy liquids. Apatites were mounted in epoxy on glass slides and ground and polished by hand. Polished grain-mounts were etched for 20 s in 5N nitric acid at 22ºC and affixed to muscovite external detectors. Samples and external detectors were stacked single-file in plastic reactor cans and irradiated in the thermal column facility at the Oregon State University TRIGA reactor. CN5 dosimetry glasses with muscovite external detectors were used as neutron flux monitors (3 per can). After irradiation, external detectors were etched in 48% HF.

Tracks were counted with a Zeiss Axioskop microscope with a 100x air objective, 1.25x tube factor, 10x eyepieces, and transmitted light with supplementary reflected light as needed. External detector prints were located with Kinetek automated scanning stage (Dumitru, 1993). Only grains with c axes subparallel to the slide plane were dated. Ages calculated using zeta calibration factor of 367.6 ± 5.0 (e.g., Hurford and Green, 1983). Ages reported are the fission-track central age of Galbraith and Laslett (1993). Confined track lengths were measured only in apatite grains with c axes subparallel to slide plane; only horizontal tracks were measured (within ±5–10°), following protocols of Laslett et al. (1982). Lengths were measured with computer digitizing tablet and drawing tube, calibrated against a stage micrometer (Dumitru, 1993). Confined track lengths were measured along with angles of tracks to the grains' c-axes, following the protocols of Ketcham et al. (1999). Confined tracks hosted by surface tracks and by cleavage surfaces were both measured. Age calculations were done with an Excel® program by J. Colgan.

Table DR1. Apatite fission-track counting data for sample WR104.

Figure DR1a. Fission-track length histogram for sample WR104.

Figure DR1b. Arcsine-weighted radial plot for sample WR104.

Table DR1: Apatite fission-track counting data for sample WR104

No	Spontaneous		Induced		$P(\chi^2)$	Dosimeter		Age ± 2σ
xls	Rho-S	NS	Rho-I	NI	(%)	Rho-D	ND	(Ma)
30	0.0840	71	1.7937	1517	46.8	1.3478	3546	11.6 ± 2.8

Abbreviations are: No xls, number of grains dated; Rho-S, spontaneous track density (x 10^6 tracks/cm^2); NS, number of spontaneous tracks; Rho-I, induced track density in muscovite external detector (x 10^6 tracks/cm^2); NI, number of induced tracks; $P(\chi^2)$, χ^2 probability (Galbraith, 1981); Rho-D, induced track density in external detector adjacent to dosimeter glass (x 10^6 tracks/cm^2); ND, number of tracks counted in determining Rho-D; Age is the central fission track age (Galbraith and Laslett, 1993), calculated using zeta calibration method (Hurford and Green, 1983) with a zeta factor of 367.6 ± 5.0. Analyst: J. P. Colgan.

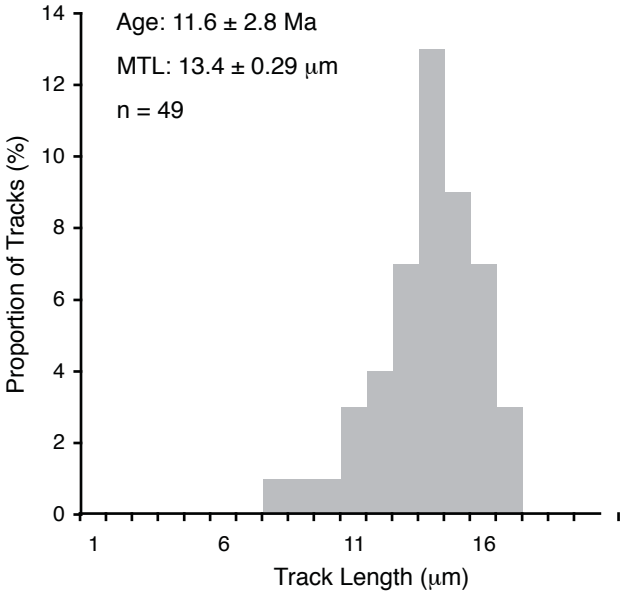

Figure DR1a. Fission-track length histogram for sample WR104. MTL is Mean Track Length.

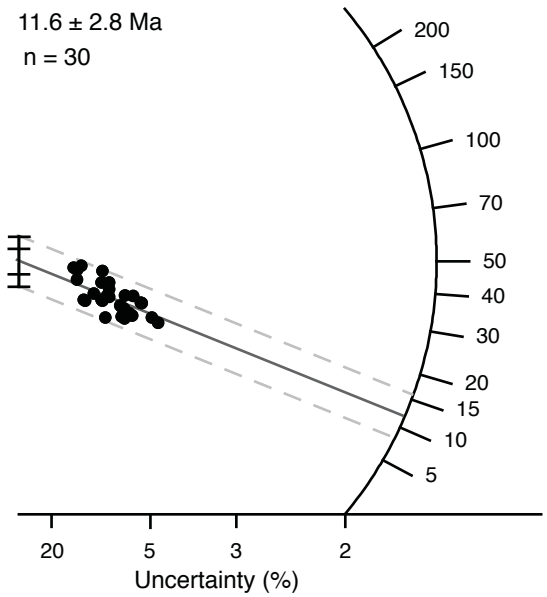

Figure DR1b. Arcsine-weighted radial plot for sample WR104 (after Galbraith and Laslett, 1993). Circular axis is age (Ma). Solid gray line is the fission-track central age; dashed gray lines are 2σ uncertainty on the central age.

(U-Th)/He thermochronometry: Methods and data

Hand-picked apatite grains were analyzed at the University of Arizona in 2007. Two grains each from samples WR104 and WR122 were previously analyzed at Yale University in 2004; these analyses were reported in Colgan et al. (2006). Both laboratories used very similar procedures; the following description applies to both unless specifically noted. Dated apatite grains were hand-picked from prepared mineral concentrates with a high-power (160x) stereo-zoom microscope with cross-polarization for screening inclusions. Individual crystals selected for analysis were digitally photographed and measured in at least 2 different orientations for alpha-ejection correction. Crystals were loaded into 1mm Pt foil tubes, which were loaded into copper or stainless steel planchets and heated with a Nd-YAG laser for 3 minutes at 1–5 W. ^{4}He blanks (0.05–0.1 fmol ^{4}He) were determined by heating empty foil packets using the same procedure.

Gas liberated from samples was processed by: 1) spiking with ~4pmol of ^{3}He, 2) cryogenic concentration at 16 K on a charcoal trap, and purification by release at 37 K, and 3) measurement of ^{4}He/^{3}He ratios (corrected for HD and H_3 by monitoring H^+) on a quadrapole mass spectrometer. All ratios were referenced to multiple same-day measured ratios and known volumes of ^{4}He standards processed in the same way. After degassing, samples were retrieved from the laser cell, spiked with calibrated ^{229}Th and ^{233}U solution, and dissolved *in-situ* from Pt tubes in ~30% HNO_3 in teflon vials. Each batch of samples was prepared with a series of acid blanks and spiked normals to check the purity and calibration of the reagents and spikes. Spiked solutions were analyzed as 0.5 mL of ~1.5 ppb U-Th solutions by isotope dilution on a Finnigan Element2 ICP-MS. Alpha-ejection was corrected using the method of Farley et al. (1996). Replicate analyses of Durango apatite (31.44 ± 0.18 Ma; McDowell et al., 2005) during the period of these analyses yielded an age of 32.8 ± 1.1 Ma (2σ, n = 3) at Yale, and 29.9 ± 0.4 Ma (2σ, n = 2) at Arizona.

Table DR2. (U-Th)/He analytical data

Figure DR2a. Age plot for sample WR104.

Figure DR2b. Age plot for sample WR122.

^{4}He/^{3}He thermochronometry: Methods and data

Approximately 30 mg of separated apatite grains were packaged into an Al foil package and irradiated with 220 MeV protons at The Francis H. Burr Proton Therapy Center at Massachusetts General Hospital. The grains were subjected to a fluence of ~5×10^{15} p/cm^2 over ~8 continuous hours in April, 2006. Following irradiation, apatite grains were hand-picked from prepared mineral concentrates using a binocular microscope to screen each crystal for mineral inclusions under crossed polarized light at 184× magnification. We binned 9 (WR104-a; Table DR3) and 5 (WR104-b; Table DR4) like-sized crystals into two sub-populations for duplicate multi-crystal ^{4}He/^{3}He analyses. The primary analysis was conducted on WR104-a, where WR104-b served as a test for internal consistency. We calculated an F_T value (Farley et al., 1996) from the geometry of each crystal measured with a calibrated micrometer and camera system attached to the microscope. The mean F_T value (0.73 ± 0.02 (2σ) and 0.78 ± 0.04, for WR104-a and WR104-b, respectively) was used to model the ^{4}He/^{3}He results for each analysis.

TABLE DR2: (U-Th)/He data

Grain number	Corrected Age (Ma)	± 2σ (Ma)[1]	Ft[2]	radius (μm)	mass (μg)	U (ppm)	Th (ppm)	U/Th	He (nmol/g)
Grains analyzed at Yale University (2004), reported in Colgan et al. (2006)									
Y-WR104a	3.28	0.20	0.69	42	2.4	20.5	29.3	0.7	0.33
Y-WR104b	3.16	0.19	0.78	61	7.2	16.7	25.9	0.6	0.30
Y-WR122a	3.00	0.80	0.71	43	2.8	3.4	5.1	0.7	0.05
Y-WR122b	2.00	0.10	0.82	76	12.9	3.0	6.9	0.4	0.04
DUR1 (std.)[3]	33.08	0.67	n/a	n/a	-	-	-	-	-
DUR2 (std.)[3]	31.70	0.64	n/a	n/a	-	-	-	-	-
DUR2 (std.)[3]	33.64	0.65	n/a	n/a	-	-	-	-	-
Grains analyzed at the University of Arizona (2007), this study									
A-WR104a	3.93	0.18	0.73	52	4.0	18.9	28.2	0.7	0.40
A-WR104b	2.44	0.13	0.73	53	4.4	16.9	24.7	0.7	0.22
A-WR104c	2.96	0.13	0.73	53	4.0	19.7	27.0	0.7	0.30
A-WR104e	3.11	0.16	0.67	42	2.1	29.1	42.5	0.7	0.44
A-WR122a	2.02	0.12	0.82	82	14.5	3.5	6.6	0.5	0.05
A-WR122b	4.00	0.22	0.75	57	5.5	4.8	11.8	0.4	0.13
A-WR122c	1.99	0.13	0.79	70	9.3	3.9	8.2	0.5	0.05
DUR1 (std.)[3]	30.00	0.61	n/a	n/a	-	-	-	-	-
DUR2 (std.)[3]	29.83	0.60	n/a	n/a	-	-	-	-	-
WR104-a[4]	3.03	0.31	0.72	52	34.0	18.7	29.9	0.6	0.31
WR104: Average[5]	3.12	0.20		50		20.3	29.6		

[1]Analytical precision only

[2]Ft is the alpha-ejection correction of Farley et al. (1996)

[3]Durango apatite with an assumed age of 31.44 ±0.18 Ma (McDowell et al., 2005)

[4]Packet of 9 grains analyzed by the $^4He/^3He$ method (table DR3)

[5]Used for He model in HeFTy (Figures 3 and 5 of the text)

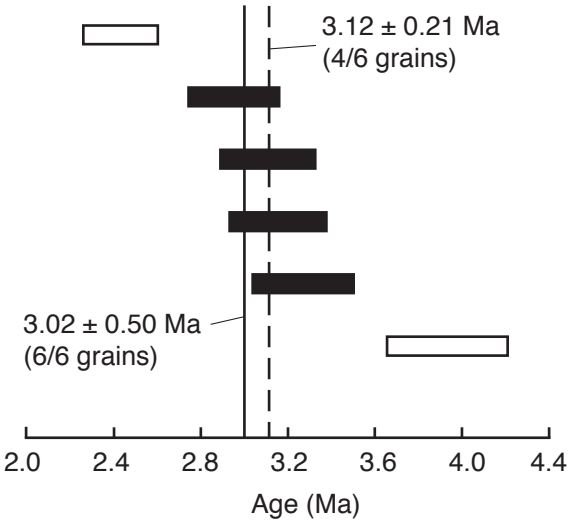

Figure DR2a. Single-grain (U-Th)/He ages of sample WR104 (bars are 2σ analytical uncertainty). Dashed line is weighted-mean age of a subset of grains (black); solid line is weighted-mean age of all grains.

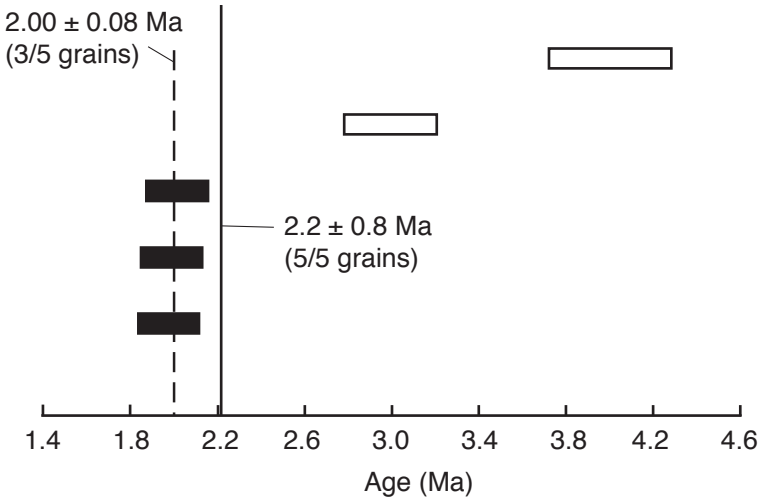

Figure DR2b. Single-grain (U-Th)/He ages of sample WR122 (bars are 2σ analytical uncertainty). Dashed line is weighted-mean age of a subset of grains (black); solid line is weighted-mean age of all grains.

$^4He/^3He$ stepped heating analyses were conducted at the Noble Gas Thermochronometry Laboratory at Berkeley Geochronology Center. We wrapped each aliquot in ~3 mm^3 of Mo foil and loaded each onto a thin-wire (0.13 mm gauge) type-K thermocouple under ultra-high vacuum. The samples were heated to better than ±2 ^oC (2σ over heating duration, typically 0.5 hr) at all set point temperatures using a projector light bulb below 400 ^oC as an external heat source (Farley, et al., 1999) and a 30 W diode laser (λ = 810 nm) above 400 ^oC. The output of each heat source was controlled in feedback with the thermocouple output using PID temperature controllers. Set point temperatures were exceeded by no more than 5 ^oC at each heating step. After each heating step, the evolved gas was automatically expanded into a pneumatically controlled, ultra-high vacuum system for (i) purification through exposure to a ST-101 alloy, reactive SAES GP-50 getter pump, and (ii) separated from other noble gases by first adsorbing the purified gas onto activated charcoal held at 12 K, then releasing pure helium at 33 K. The helium was then expanded into an automated MAP 215-50 mass spectrometer for analysis. Both ^3He and ^4He were measured on a continuous dynode electron multiplier with sufficient mass resolution to completely resolve ^3He from the HD-H_3 composite peak using pulse-counting electronics.

The instrument sensitivity and response linearity was monitored by analyzing different sized pipettes of a working helium standard with $^4He/^3He$ = 1538 ± 10. The number of moles of ^4He delivered by each standard pipette was known to better than ± 0.5%; the volumes of the pipettes and standard tank were ultimately calibrated against a gravimetrically determined Pyrex volume. We used the diode laser as a heat source primarily to minimize ^4He blanks (the laser heating minimizes the heating of the vacuum chamber walls), which averaged 19 ± 1.8 × 10^6 atoms over the course of each analysis (typically 10% of the measured ^4He at each step and the dominant source of uncertainty in each $^4He/^3He$ measurement). After approximately every 8^{th} heating step, a room temperature procedural blank and a working standard was analyzed. Analytical uncertainty in the ^4He and ^3He blanks (estimated from the reproducibility of all blanks measured over the course of each stepwise heating analysis) and the heating step measurements were fully propagated into the reported $^4He/^3He$ ratios and ^3He concentrations shown in the supplementary tables (DR3 and DR4).

Table DR3: $^4He/^3He$ analytical data for packet WR104-a

Figure DR3a. $^4He/^3He$ ratio evolution diagram for packet WR104-a

Figure DR3b. Model residuals for packet WR104-a

Table DR4: $^4He/^3He$ analytical data for packet WR104-b

Figure DR4. $^4He/^3He$ ratio evolution diagram for packet WR104-b.

Table DR3: He/He step-heating data for WR104-a

Step	T (^{o}C)	t (hr)	[^{3}He] (Matom)	(+/-) 2σ	R/R_{bulk}	(+/-) 2σ
1	240	0.54	1.22	0.07	0.316	0.056
2	260	0.46	1.22	0.08	0.499	0.089
3	270	0.43	1.25	0.07	0.543	0.081
4	270	0.60	1.31	0.09	0.564	0.089
5	280	0.48	1.17	0.07	0.610	0.097
6	280	0.60	1.30	0.08	0.559	0.089
7	290	0.42	1.20	0.06	0.664	0.092
8	290	0.49	1.28	0.08	0.812	0.115
9	310	0.43	2.08	0.10	0.771	0.054
10	310	0.56	2.91	0.12	0.697	0.031
11	320	0.42	2.48	0.11	0.746	0.042
12	320	0.52	1.74	0.09	0.992	0.088
13	320	0.63	2.15	0.10	0.901	0.055
14	330	0.47	1.99	0.09	0.914	0.060
15	330	0.56	2.26	0.09	0.937	0.049
16	330	0.66	2.08	0.09	1.011	0.063
17	340	0.50	1.86	0.10	1.112	0.091
18	340	0.61	2.03	0.10	1.102	0.077
19	350	0.47	2.14	0.08	1.032	0.055
20	350	0.60	2.22	0.10	1.132	0.067
21	360	0.51	2.40	0.10	1.114	0.057
22	370	0.48	2.68	0.12	1.161	0.055
23	380	0.50	3.51	0.14	1.059	0.035
24	380	0.50	2.85	0.13	1.098	0.049
25	390	0.50	3.34	0.15	1.070	0.041
26	400	0.50	3.55	0.15	1.070	0.037
27	400	0.50	2.81	0.11	1.088	0.045
28	410	0.50	2.80	0.11	1.219	0.051
29	410	0.50	2.36	0.11	1.135	0.065
30	420	0.50	2.53	0.13	1.130	0.067
31	420	0.50	2.31	0.11	1.047	0.062
32	440	0.50	2.44	0.11	1.141	0.063
33	460	0.50	2.81	0.13	1.137	0.053
34	520	0.50	3.92	0.15	1.206	0.033
35	560	0.50	1.89	0.09	1.298	0.095
36	600	0.50	1.10	0.07	1.250	0.198
LS	1100	0.25	2.11	0.07	1.121	0.170

R_{bulk} = 76.292

Matom = 10^{6} atoms

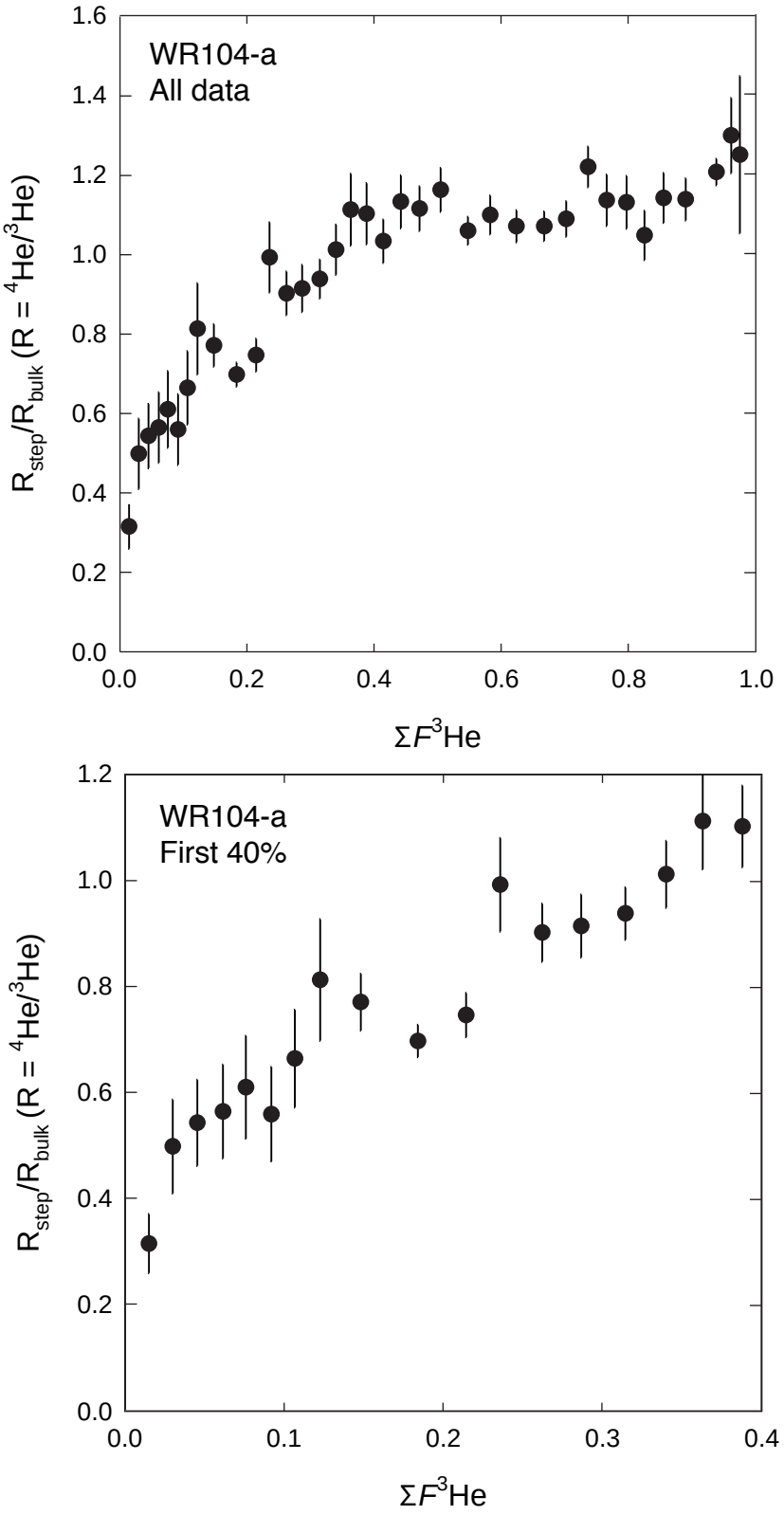

Figure DR3a. $^4He/^3He$ ratio evolution diagram for sample WR104-a.

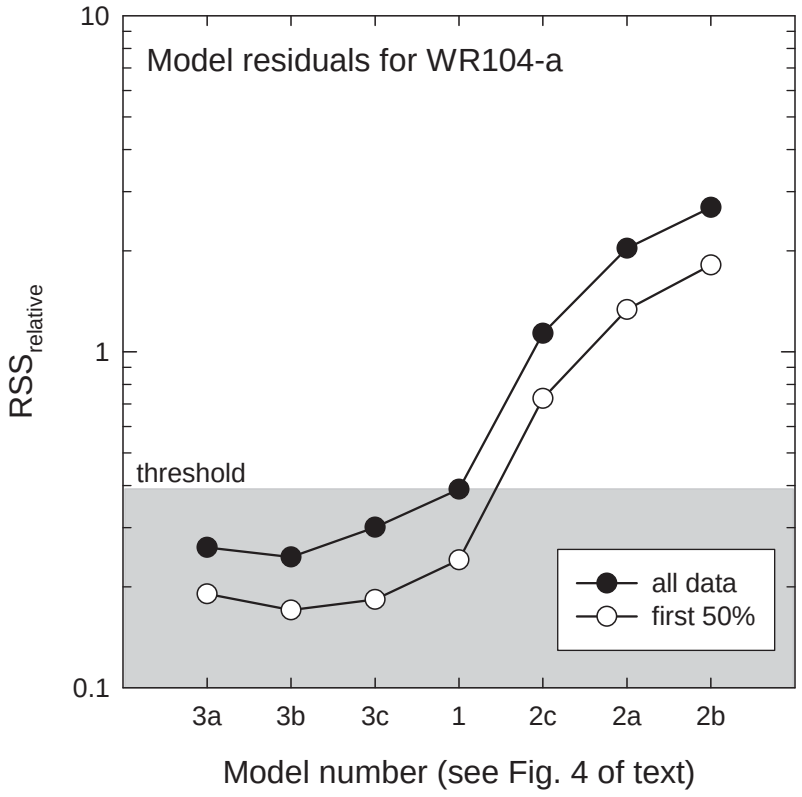

Figure DR3b. Model residuals for sample WR104-a. Numbers correspond to *t-T* paths in Figure 4 of the text. RSS is Residual Sum of Squares.

Table DR4: He/He step-heating data for WR104-b

Step	T (^{o}C)	t (hr)	[^{3}He] (Matom)	(+/-) 2σ	R/R_{bulk}	(+/-) 2σ
1	240	0.54	0.69	0.06	0.37	0.16
2	260	0.46	0.67	0.06	0.45	0.20
3	270	0.43	0.64	0.06	0.59	0.25
4	270	0.60	0.59	0.05	0.69	0.33
5	280	0.48	0.55	0.06	0.62	0.37
6	280	0.60	0.60	0.05	0.74	0.33
7	290	0.42	0.56	0.05	0.76	0.38
8	290	0.49	0.62	0.06	1.12	0.49
9	310	0.43	1.10	0.08	0.83	0.16
10	310	0.56	1.09	0.07	0.86	0.15
11	320	0.42	1.21	0.07	0.79	0.11
12	320	0.52	1.24	0.09	0.95	0.15
13	320	0.63	1.07	0.07	1.12	0.21
14	330	0.47	1.16	0.07	1.05	0.17
15	330	0.56	1.08	0.07	0.95	0.17
16	330	0.66	1.27	0.07	1.17	0.14
17	340	0.50	1.24	0.07	0.95	0.13
18	340	0.61	1.36	0.08	1.01	0.13
19	350	0.47	1.14	0.07	1.03	0.17
20	350	0.60	1.47	0.09	1.08	0.12
21	360	0.51	1.46	0.08	1.08	0.12
22	370	0.48	1.53	0.09	1.13	0.12
23	380	0.50	1.93	0.10	1.23	0.09
24	380	0.50	1.60	0.10	1.12	0.12
25	390	0.50	2.01	0.10	1.07	0.07
26	400	0.50	2.27	0.10	1.06	0.06
27	400	0.50	1.85	0.10	1.08	0.09
28	420	0.50	3.33	0.13	1.07	0.04
29	420	0.50	2.63	0.12	1.08	0.05
30	440	0.50	2.26	0.11	0.96	0.06
31	460	0.50	3.05	0.13	1.06	0.07
32	480	0.50	2.18	0.10	0.95	0.06
33	500	0.50	1.23	0.08	0.98	0.15
34	520	0.50	0.66	0.06	1.03	0.39
LS	1100	0.25	1.58	0.10	0.96	0.13

R_{bulk} = 79.77

Matom = 10^{6} atoms

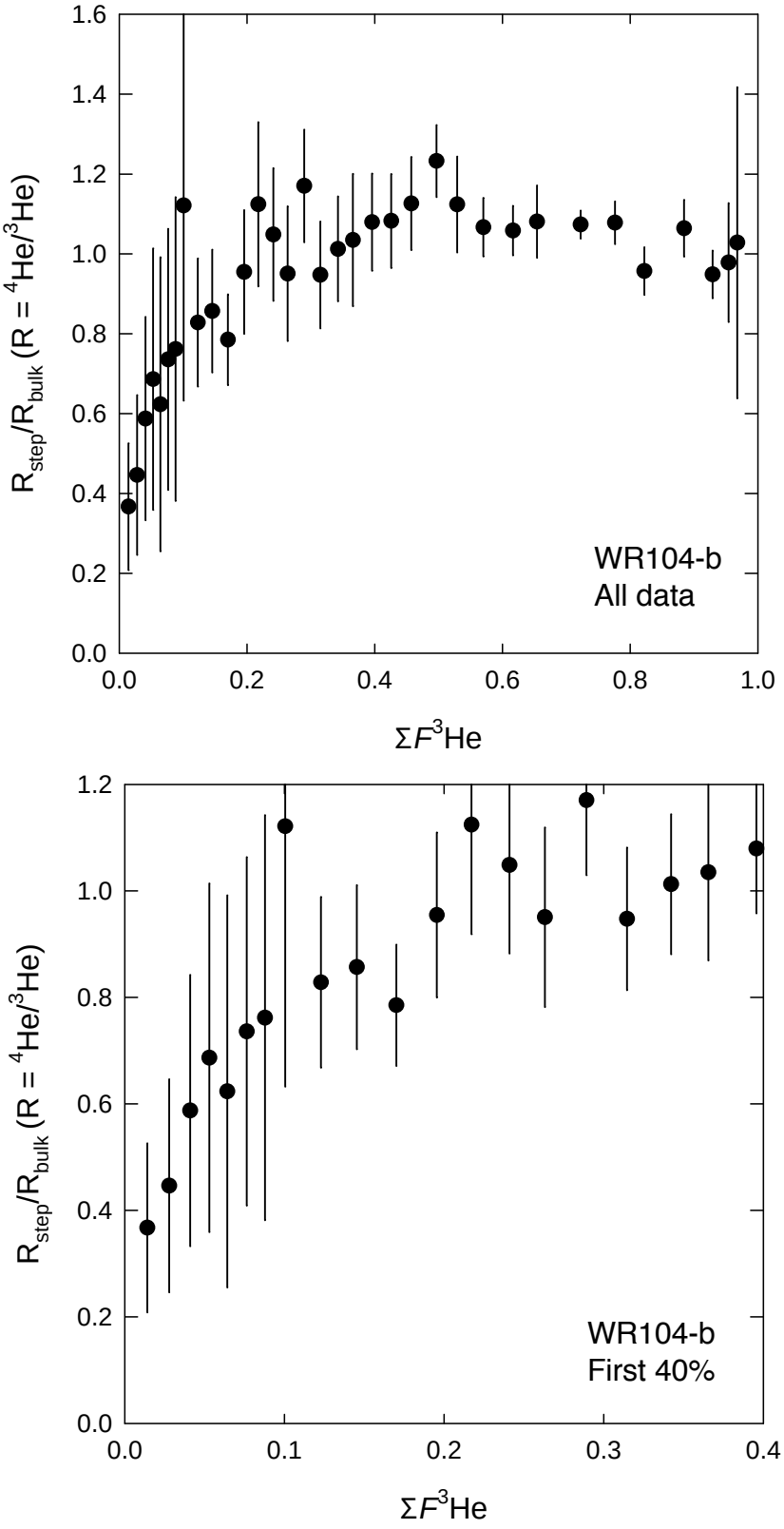

Figure DR4. $^4He/^3He$ ratio evolution diagram for sample WR104-b.

Description of thermal modeling parameters

For the thermal models shown in Figures 3 and 5, the HeFTy (v. 1.4) search algorithm of Ketcham (2005) was used with the following parameters:

For the (U-Th)/He model: Diffusion model: Shuster et al., 2006 (Do/a^2); Radius: 50 μm; Alpha calculation: Static ejection; Anneal traps: He Loss; U concentration = 20 ppm; Th concentration = 30 ppm; Measured age (uncorrected): 2.12 ± 0.35, yielding a corrected age of 3.03 ± 0.50 Ma; Age alpha correction: Ketcham, in prep.

For the fission-track model: Annealing model: Ketcham et al. (1999); C-axis projection: Donelick et al. (1999), Default initial track length: From Dpar; Kinetic parameter: Dpar (sample treated as a single kinetic population with a mean Dpar of 2.44 from a range of 1.98–2.91); [Age] Uncertainty mode: 95% ±; GOF Method: Kuiper's statistic.

For Figure 3, the model was run with the following parameters: Search Method: Monte Carlo; Subsegment spacing: Random; Ending condition: Good Paths = 200; Merit value for good fit (0.5); Merit value for acceptable fit (0.05). The single segment from 14 to 0 Ma was split two times.

For Figure 5, the model was run with the following parameters: Search Method: Monte Carlo; Subsegment spacing: Random; Ending condition: Good Paths =200; Merit value for good fit (0.5); Merit value for acceptable fit (0.05). The segment from 14 to 4.5 Ma was split 2 times; the younger segments were each split 0 times.

SHRIMP U-Pb geochronology: Methods and data

Zircon concentrates were prepared at Stanford University using standard mineral separation techniques and handpicked under a binocular microscope to ensure purity. At the Stanford - U.S.G.S. Micro Analytical Center (SUMAC), the selected grains were mounted in epoxy with the laboratory standard zircon R33 (419 Ma; Black et al., 2004) and polished with diamond compound to expose the mid-points of the crystals. Polished grain mounts were imaged in reflected light with an optical microscope, gold-coated, and imaged in cathodoluminescence (CL) mode with a JEOL 5600 scanning electron microscope.

The SHRIMP-RG ion microprobe at SUMAC was operated with an O_2^- primary ion beam varying from 4 to 6 nA, which produced a spot with a diameter of ~20–30 μm and a depth of 1–2 μm on the target zircons. Eleven peaks were measured sequentially for 10 min with an ETP electron multiplier (Zr_2O, ^{204}Pb, ^{206}Pb, ^{207}Pb, ^{208}Pb, ^{238}U, ThO, UO, ErO, YbO, and HfO). Data was reduced following the methods described by Ireland and Williams (2003), using the SQUID and IsoPlot programs of Ludwig (2001, 2003).

Table DR5, U-Pb isotopic data

Figure DR5, Inverse-concordia diagram for sample WR104.

Table DR5: U-Pb SHRIMP Data

Spot name	comm 206 (%)	U (ppm)	Th (ppm)	$^{232}Th/^{238}U$	$^{206}Pb/^{238}U$ Age* (Ma, ±1 σ)	Total $^{238}U/^{206}Pb$ (± % err)	Total $^{207}Pb/^{206}Pb$ (± % err)
JC04-WR104: Warner Range							
WR104-1	0.03	350	248	0.73	108.1 ± 1.0	59.1 ± 0.9	0.0484 ± 4.7
WR104-2	-0.05	152	80	0.54	110.3 ± 1.6	58.0 ± 1.4	0.0478 ± 5.1
WR104-3	-0.21	249	156	0.65	108.3 ± 1.2	59.2 ± 1.1	0.0465 ± 4.0
WR104-4	0.11	326	222	0.70	109.6 ± 1.1	58.3 ± 0.9	0.0491 ± 3.4
WR104-5	-0.04	240	146	0.63	110.4 ± 1.2	57.9 ± 1.1	0.0479 ± 3.9
WR104-6	-0.26	377	276	0.76	111.3 ± 1.2	57.6 ± 1.0	0.0462 ± 3.4

*^{207}Pb corrected

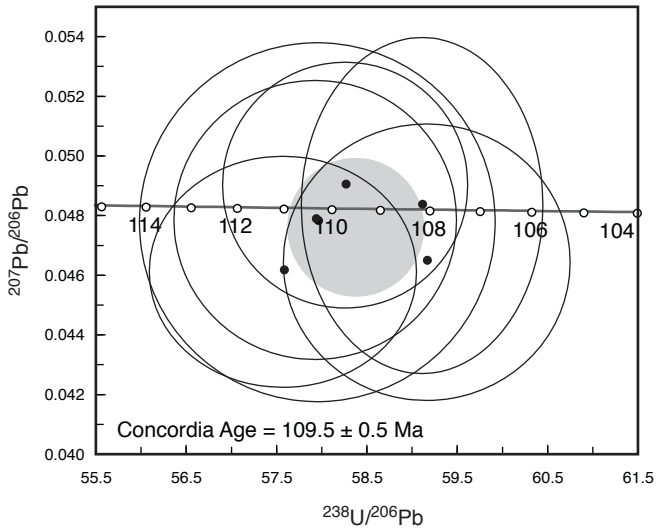

Figure DR5. Inverse concordia plot for SHRIMP U-Pb data zircon analyses from sample WR104 (6 grains total). Reported age is the "Concordia Age" (gray circle) calculated with IsoPlot (Ludwig, 2000). Error ellipses are 2σ.

DATA REPOSITORY REFERENCES

Black, L.P., Kamo, S.L., Allen, C.M., Davis, D.W., Aleinikoff, J.N., Valley, J.W., Mundil, R., Campbell, I.H., Korsch, R.J., Williams, I.S., and Foudoulis, C., 2004, Improved $^{206}Pb/^{238}U$ microprobe geochronology by the monitoring of a trace-element-related matrix effect: SHRIMP, ID-TIMS, ELA-ICP-MS, and oxygen isotope documentation for a series of zircon standards: Chemical Geology, v. 205, p. 115–140.

Colgan, J.P., Dumitru, T.A., Reiners, P.W., Wooden, J.L., and Miller, E.L., 2006, Cenozoic tectonic evolution of the Basin and Range Province in northwestern Nevada: American Journal of Science, v. 306, p. 616-654.

Donelick, R.A., Ketcham, R.A., and Carlson, W.D., 1999, Variability of apatite fission-track annealing kinetics: II. Crystallographic orientation effects: American Mineralogist, v. 84, p. 1224–1234.

Dumitru, T.A., 1993, A new computer-automated microscope stage system for fission-track analysis: Nuclear Tracks and Radiation Measurements, v. 21, p. 575-580.

Hurford, A.J., and Green, P.F., 1983, The zeta age calibration in fission-track dating: Chemical Geology, v. 41, p. 285-317.

Farley, K.A., Wolf, R.A., and Silver, L.T., 1996, The effects of long alpha-stopping distances on (U-Th)/He ages: Geochimica et Cosmochimica Acta, v. 60, p. 4223–4229.

Farley, K., Reiners, P., and Nenow, V., 1999, An apparatus for high-precision helium diffusion measurements from minerals: Analytical Chemistry, v. 71, p. 2059–2061.

Galbraith, R.F., and Laslett, G.M., 1993, Statistical models for mixed fission-track ages: Nuclear Tracks and Radiation Measurements, v. 21, p. 459-470.

Hurford, A.J., and Green, P.F., 1983, The zeta age calibration in fission-track dating: Chemical Geology, v. 41, p. 285–317.

Ireland, T.R., and Williams, I.S., 2003, Considerations in zircon geochronology by SIMS: *in* Hanchar, J.M., and Hoskin, P.W.O., eds., Zircon: Mineralogical Society of America and Geochemical Society. Reviews in Mineralogy and Geochemistry, v. 53, p. 215–241.

Ketcham, R.A., Donelick, R.A., and Carlson, W.D., 1999, Variability of apatite fission-track annealing kinetics. 3. Extrapolation to geological time scales: American Mineralogist, v. 84, p. 1235–1255.

Ketcham, R.A., 2005, Forward and inverse modeling of low-temperature thermonometry data, *in* Reiners, P.W., and Ehlers, T.A., eds., Low-temperature thermochronology: Techniques, interpretations, and applications: Reviews in Mineralogy and Geochemistry, v. 58, p.275–314.

Laslett, G.M., Kendall, W.S., Gleadow, A.J.W., and Duddy, I.R., 1982, Bias in the measurements of fission-track length distributions: Nuclear Tracks and Radiation Measurements, v. 6, p. 79–85.

Ludwig, K.R., 2001, Squid: A users' manual: Berkeley Geochronology Center Special Publication 2, 19 p.

Ludwig, K.R., 2003, Isoplot 3.00, a geochronological tool-kit for Excel: Berkeley Geochronology Center Special Publication 4, 67 p.

McDowell, F.W., McIntosh, W.C., and Farley, K.A., 2005, A precise $^{40}Ar/^{39}Ar$ reference age for the Durango apatite (U-Th)/He and fission-track dating standard: Chemical Geology, v. 214, p. 249–263.

Shuster D.L., Flowers R.M., Farley K.A., 2006, The influence of natural radiation damage on helium diffusion kinetics in apatite: Earth and Planetary Science Letters, v. 249, p. 148–161.